Ultrafine and Fairly Long Carboxylated Cellulose Nanofibers Prepared by a Hydrated Multi-carboxylic Acid Deep Eutectic Solvent

Xiaochao Shi
Northeast Forestry University

Zengbin Wang
University of Göttingen

Qinqin Xia
Northeast Forestry University

Yongzhuang Liu
Northeast Forestry University

Wenshuai Chen
Northeast Forestry University   https://orcid.org/0000-0003-4428-1505

Haipeng Yu
Northeast Forestry University   https://orcid.org/0000-0003-0634-7913

Kai Zhang (✉ kai.zhang@uni-goettingen.de)
Georg-August-University of Göttingen   https://orcid.org/0000-0002-5783-946X

Article

Additional Declarations: There is **NO** Competing Interest.

Abstract

Sustainable carboxylated cellulose nanofibers (C-CNFs) with access to variable surface chemical modifications and exquisite mechanical properties have great and promising applicability across various fields. However, the current fabrication processes either require harsh reaction conditions or severely impair the high aspect ratio of products, resulting in low yields, environmental issues and/or limited uses. Herein, we address these limitations by using a hydrated multi-carboxylic acid deep eutectic solvent comprised of only choline chloride, citric acid, and water to produce ultrafine and fairly long C-CNFs. The resultant C-CNFs have fine diameters of ~ 3 nm, high aspect ratios up to 4000, high carboxyl content of 1.5 mmol/g, and high yield of 90%. Notably, we can easily achieve large-scale production of C-CNFs for preparing large area, high-performance structural materials. Superior stability of the C-CNFs suspensions even at high concentrations allows the fabrication of 4 m-long flexible C-CNF films showing excellent mechanical strength, great optical properties (92% transparency and 90% haze) and high thermal stability (T_{max}=348 °C) as well as of large area C-CNF aerogels with ultralow bulk density of 0.002 g/cm^3, ultrahigh porosity of 99.86% and super low thermal conductivity of 0.0289 W/mK. These unique advantages as high yield, great cost-efficiency, scalable productivity and recyclability of eutectic solvents open up a new route to producing ultrafine C-CNFs on an industrial scale.

Introduction

Cellulose nanofibers (CNFs) are widely present in living organisms (e.g., wood, bamboo, straw, pulp, grass, tunicate) in nature as nanostructures. They have extraordinary physicochemical and biologic qualities due to their well-defined molecular structures and geometries, allowing them to perform a range of particular activities in biological systems and serve as building blocks in material science.[1−4] From a bionic perspective, CNFs exhibit great potential for the development of sustainable multifunctional biocomposites due to their natural abundance, unique nanostructure, high mechanical and thermal stability, and excellent biocompatibility.[5] However, the elementary cellulose nanofibrils are difficult to utilize due to their likely to aggregate and inability to be stably dispersed in suspensions. The most typical method is to use chemical processes to exfoliate the nanofibrils and increase the concentration of carboxyl groups on the nanofibrils' surfaces, resulting in ultrafine and carboxylated cellulose nanofibers (C-CNFs).[6] C-CNFs with fine diameter, slim morphology and functional groups can overcome the weak dispersibility in aqueous solution, and achieve stable dispersion through electrostatic repulsions.[7]

The top-down preparation method is the most recognizable and widely used procedure of C-CNFs due to its superiority in maintaining nanofibrous morphology. These methods combine partly surface ionization of raw materials with external mechanical treatments such high-pressure homogenization, ball milling, and ultrasonic nanofibrillation. The most famous and successful case of producing C-CNFs from cellulose is using 2,2,6,6-tetramethyl-1-piperidinyloxy (TEMPO)-mediated oxidation via regioselective conversion of cellulose C$_6$ hydroxyl groups to carboxyl groups.[8] The negatively charged carboxylate entities promote the disintegration of nanofibrils and the formation of homogeneous and stable

suspensions due to electrostatic repulsion.[9] However, this process suffers from expensive reagents, a pH-dependent reaction, long processing time, and environmental issues such as harmful gas emissions and waste liquids.[10] Another frequently-used method to produce C-CNFs is acid-catalyzed esterification (termed as Fischer esterification) using various organic acids.[11-12] However, although having high carboxyl contents, such C-CNFs suffer from deficiencies such as low aspect ratios (several dozens), low yields (20–60%), and decreased degree of polymerization (DP: ~300). There exhibits a contradiction between high carboxyl content and high aspect ratio. Therefore, the C-CNFs production has long been limited by harsh reaction conditions or the instability of suspensions, which led to low production yield that prevents large-scale production. Large-scale preparing C-CNFs with both high carboxyl content and high aspect ratio in a green and cost-efficient way is believed to be challenging but desirable.

Herein, we describe a facile method for producing ultrafine and fairly long C-CNFs with high carboxyl contents in high yields using a green and low-cost hydrated multi-carboxylic acid deep eutectic solvent (designated as H-DES) composed of citric acid (CA), choline chloride (ChCl) and water. The tailored H-DES is capable of breaking the hydrogen bonds (H-bonds) of cellulose while simultaneously grafting carboxyl groups (Fig. 1a). Thereby, CA as a kind of tricarboxylic acid allows H-DES to contain multi-carboxyl acid groups for grafting onto cellulose, the steric hindrance of ChCl prevents the formation of cyclic anhydride and preserves more carboxyl sites, and water as an H-DES component regulates the protonation properties of the solvent to avoid excessive hydrolysis of cellulose. Therefore, the resultant C-CNFs not only exhibit high aspect ratios and rich carboxyl groups, but also inherit the native attributes of cellulose, including high DP, large amount of crystalline domains and high thermal stability. More significantly, the moderate reaction conditions of C-CNFs enable the upscaling of the manufacturing process with large-scale equipment. As shown in Fig. 1b, the C-CNFs produced by the H-DES are comprehensively superior to those prepared by TEMPO-mediated oxidation and organic acid/anhydride treatments. Therefore, this work enables the economic and environmentally friendly production of ultrafine C-CNFs with high aspect ratios and abundant carboxyl groups.

Results And Discussion

Fabrication of ultrafine C-CNFs

Mass producible and affordable bleached pulp was selected as the starting material to prepare the unmodified CNFs and objective C-CNFs via the combination of chemical pretreatment and the mechanical nanofibrillation process. Generally, the CNFs from $NaClO_2$ and KOH pretreatment do not have uniformly fine diameters and high zeta potentials and are then incapable of forming a homogeneous and long-standing stable suspension (Figure 2a-c). To pretreat bleached pulp to fabricate the objective C-CNFs, tailored H-DESs composed of CA (H-bond donor), ChCl (H-bond acceptor), and water (proton regulating agent) were designed and synthesized. Using the aspect ratio, carboxyl content, and yield of C-CNFs as evaluation indicators, various combinations of H-DES components in different ratios were tested to obtain an optimal formula. Results show that obtained C-CNFs exhibit finer diameters and higher carboxyl content with increasing molar ratio of CA to ChCl (Figure S1). Meanwhile, the C-CNFs

suspension becomes more transparent, showing improved homogeneity and dispersion stability (Figure 2d). Note that excessive CA would cause excessive hydrolysis of cellulose, which results in a reduction in the length and DP of C-CNFs (Figure S1). For example, the lengths of C-CNFs from anhydrous DES (CA:ChCl=4:1) are shortened to around 1 μm. Therefore, the mass ratio of CA:ChCl at 3:1 is deemed an optimal ratio of these two components. The C-CNFs prepared with such a solvent show fine diameters of ~3 nm and good dispersibility (Figure 2e,f).

By adding an appropriate amount of water, the cost, H-bond acidity, and viscosity of H-DES can be reduced while maintaining C-CNF lengths greater than 2 μm, and the optimal mass ratio of CA:ChCl:H_2O is determined to be 3:1:1 (Figure S2). The C-CNFs (Figure 2g-i) prepared with this solvent display more uniform and finer diameters and higher carboxyl content than the unmodified CNFs, and are comparable to those of the C-CNFs (Figure 2d-f) prepared with the anhydrous DES (CA:ChCl=3:1). The C-CNFs prepared in this condition also generate a high yield of 90%. The C-CNFs are primarily composed of single elementary fibers which show the statistically finest fiber diameter of 2.5 nm, longest fiber length of 10 μm, and highest aspect ratio of 4000 (Figure 2j). Three distinct peaks at 2θ = 16.2, 22.6, and 34.6, corresponding to the (110), (200), and (004) crystalline planes, are visible in all samples, indicating that the cellulose I crystalline structure was preserved following H-DES treatment (Figure S3). Therefore, the desired C-CNFs with high yield were successfully fabricated under the synergistic regulation of H-DES and subsequent ultrasonic nanofibrillation treatments.

Fourier transform infrared (FTIR) spectroscopy analysis reveals the reason for the high carboxylation rate of C-CNFs (Figure S4). Two adjacent carboxylic groups of CA are easily dehydrated to form the five-membered cyclic carboxylic anhydride,[13] which has a negative effect on the carboxylation rate of cellulose. However, no cyclic carboxylic anhydride is detected in the FTIR spectrum of H-DES. We presume that the existence of ChCl featured with a CH_2OH chain extending from one of the vertices can generate a steric hindrance effect, which hinders the formation of cyclic carboxylic anhydride. In this condition, more free carboxylic groups grafted to the cellulose improve the carboxylation rate of C-CNFs. Therefore, the C-CNFs prepared by the optimized H-DES have a high carboxyl content of 1.5 mmol/g (Figure S5), which is higher than most of the reported values in literature, while the width, length, and yield of C-CNFs are simultaneously far above those obtained by TEMPO-mediated oxidation and organic acid treatments (Figure 3a-c). Zeta potential is mainly associated with the carboxyl content of C-CNFs, and the zeta potential value of C-CNFs prepared using the optimized H-DES was about −47 mV, exceeding most of those achieved by conventional methods (Figure 3d). High carboxyl content and zeta potential are beneficial to the dispersion stability of C-CNFs in aqueous solution.

Chemical characteristics of C-CNFs

We further investigated the chemical structures of C-CNFs using a series of spectroscopic methods. In the Raman spectrum of C-CNFs, a new absorption peak at 1740 cm^{-1} corresponding to the carbonyl group (C=O) appears in Figure 4a, indicating the grafting of carboxyl groups onto CNFs. The Raman mapping images show that only hydroxyl groups (O-H) can be detected from the CNFs (Figure 4b), whereas

hydroxyl groups and carbonyl groups (C=O) are manifested clearly from the C-CNFs (Figure 4c), demonstrating homogeneous distribution of carboxyl groups in the C-CNFs.[32] X-ray photoelectron spectroscopy (XPS) confirms the chemical structure and state changes of C/O elements (Figure 4d). The C/O ratio of C-CNFs is higher than that of CNFs, suggesting that a plenty of carbon-oxygen groups has been grafted. Therefore, the C-CNFs have a new carbon atom binding form of O-C=O at 287.8 eV, compared to CNFs (Figure 4e,f). The signal of C=O stretching of carboxyl groups at 1735 cm^{-1} also appeared in the FTIR spectrum (Figure 4g). Furthermore, various C=O forms of the ester group (C7), methylene group (C8, C8*), quaternary carbon atom (C9), and carboxyl group (C10) are further revealed by ^{13}C NMR spectroscopy (Figure 4h), proving the conjectural linkage structure.

The esterification of carboxyl groups onto cellulose leads to the crosslinking of C-CNFs. The degree of crosslinking can be assessed by the ratio of free carboxyl content (FCC) to total carboxyl content (TCC).[18] FCC is the number of free carboxyl groups, TCC is the total number of free carboxyl groups (-COOH) and bonded carboxyl/ester groups (O-C=O) of CA.[17] Ideally, only one carboxyl group of CA is esterified with cellulose, while the other two carboxyl groups remain free, and the FCC/TCC ratio under this condition is 2/3 (Figure S6), which indicates that no crosslinking has occurred. The FCC/TCC ratio of C-CNFs in this experiment is so close to this ideal value, which suggests that scarcely any crosslinking occurred between C-CNFs.

Physical and mechanical properties of C-CNFs

As shown in Figure 5a, freestanding and flexible films consisting of interwoven C-CNFs can be fabricated through a facile solution casting method. In comparison to conventional CNF and TEMPO-oxidized CNF films, the C-CNF film exhibits higher transmittance of 92% at 600 nm (Figure 5b) while maintaining good haze of 90% (Figure 5c), suggesting its use as a substrate material in emerging flexible electronics and optoelectronics.[33-34] The C-CNF film has excellent mechanical properties, with a tensile strength of 115.4 MPa, which is 5.5 times higher than that of a CNF film (Figure 5d). The toughness, modulus, and elongation of the C-CNF film are 17.2, 4.5, and 3.2 times higher than those of the CNF film, respectively (Figure 5e,f). The C-CNFs with high aspect ratio and high charge also show superiority in preparing aerogels, and an aerogel made of 0.2 wt% C-CNFs shows ultralow bulk density of 0.002 g/cm^3, high porosity of 99.86% (Figure 5g), superlow thermal conductivity (0.0289 W/mK, Figure 5h) close to air (0.025 W/mK), and outstanding compressive robustness (Figure 5i). Thermogravimetric analysis (TGA) reveals that C-CNFs has a thermal degradation temperature (T_{max}=348 °C) close to pristine cellulose (Figure S7). In addition, the co-existence of H-bonds and ester bonds between C-CNFs makes the C-CNF film/aerogel easily recyclable and rebuilt. The disposable C-CNF film/aerogel can be redispersed in water to become a uniform slurry and reformed into various types of products (Figure S8).

Scalable productivity of C-CNFs and derived materials

The preparation process of C-CNFs can be enlarged to a production scale of 100 L per batch (Figure 6a and S9), and the properties of C-CNFs from the large-scale production are almost the same as those from small-scale preparation. The C-CNFs from large-scale production can also maintain a homogeneous suspension state even after six months of storage (Figure 6b). Normally, the maximum solid content of CNFs is below 2 wt% (Figure 6c), while the maximum solid content of C-CNFs in this work reaches 10 wt% due to rich negative charges. The C-CNFs at 10 wt% solid content display a very fine and milky gel appearance (Figure 6d and Figure S10), with no obvious agglomerates observed. The production of such high solid content of C-CNFs can reduce the reagent cost and energy consumption, as well as facilitate the transportation. The H-DES used in this study to produce C-CNFs can be recycled and reused, which brings an economical and efficient advantage. Even after four cycles, the yield of C-CNFs is still 90% and the carboxyl content is 1.42 mmol/g (Figure S11). Therefore, this method has advantages of high efficiency, large-scale production, low cost, and recyclability, which shows its potential in industrial applications.

Based on the advantages of low cost and scaling up production of C-CNFs, we are capable of fabricating their materials from the laboratory to the pilot stage and maintaining their performance without degradation. For example, we have manufactured a transparent C-CNF film with a length of 4 m (Figure 6f) by solution casting and a room temperature drying process (Figure S12),[35] and a large bulk C-CNF aerogel with dimensions of 150 cm × 25 cm × 1 cm (Figure 6e). Furthermore, as shown in the conceptual diagram in Figure 6g, the C-CNF films and aerogels and other derivatives can be produced on an industrial scale with the help of processing equipment.

Conclusion

We demonstrate that a specific solvent of H-DES is a facile and effective method to large-scale fabricate ultrafine C-CNFs with rich carboxyl groups. It is a facile and general procedure for producing ultrafine C-CNFs from bleached pulp, with clear merits of high yield (> 90%), low cost, energy efficiency, environmentally friendliness, scalable productivity, and mild conditions. The H-DES comprised of CA, ChCl, and water at a mass ratio of 3:1:1 was deemed optimal. In such a ratio, the steric hindrance effect of ChCl effectively prevented the adjacent carboxyl groups in CA from being dehydrated to cyclic anhydride to retain enough free carboxyl sites to graft onto cellulose, and water regulated the H-bond acidity to prevent over-hydrolysis of cellulose. The as-prepared C-CNFs exhibited ultrafine diameters of 3 nm, ultralong fiber length up to 10 μm, high aspect ratio up to 4000, and a high carboxyl content of 1.5 mmol/g. The C-CNFs could uniformly disperse in aqueous solution and had excellent stability for at least six months. These advantages enabled the large-scale productivity of C-CNFs, and maximum solid content of 10 wt%, which was considerably higher than existing methods and good for transportation. These C-CNFs can be utilized as new building elements not only to construct transparent films with excellent tensile strength, toughness, and elastic modulus, but also to produce aerogels displaying high porosities of 99.86%, ultralow bulk densities of 0.002 g/cm^3, and super low thermal conductivities of 0.0289 W/mK. In conclusion, this work realized the facile production of C-CNFs comparable to TEMPO

CNFs in a highly efficient, cost-effective, and environmentally friendly manner. Both the methodology and product properties were superior to those produced by conventional methods. This strategy could boost the industrial manufacturing of functional nanocellulose and be used in promising applications including but not limited to value-added nanocomposites, thermal insulation materials, and flexible electronics.

Materials And Methods

Materials and chemicals. Bleached kraft pulp from poplar wood was used as a starting material to prepare CNFs and C-CNFs. Citric acid ($\geq$ 99.5%), hydrochloric acid (36–38%), and sodium hydroxide ($\geq$ 96%) were purchased from Shanghai Maclean Biochemical Co., LTD. (Shanghai, China). Choline chloride ($\geq$ 98%) was purchased from Shanghai Aladdin Biochemical Technology Co., LTD.

Synthesis of H-DES. Citric acid, choline chloride, and water at a mass ratio of x: 1: y (x = 1, 2, 3 or 4; y = 0, 1, 2 or 3) were mixed at 80 °C for 30 min to obtain a homogeneous and transparent liquid.

Preparation of C-CNFs. Bleached kraft pulp (4.5 g) was added to 100 mL of H-DES in a round-bottom flask and heated at 130 °C with condensing reflux for 3 h. After pretreatment, the pulp was separated and washed with deionized water. The yield was calculated as the weight percentage of oven-dried pulp to the raw kraft pulp. The pretreated pulp was soaked in water at 0.5 wt% content and then ultrasonically nanofibrillated into C-CNFs using an ultrasonic generator (JY99-IIDN, Scientz Biotechnology Co. Ltd., Ningbo, China); frequency: 20 kHz, power: 800 W, and processing time: 30 min.

During the scaling up production of C-CNFs, bleached kraft pulp was pretreated in 14 L H-DES in a 16-L volume digester and heated at 130 °C for 3 h. Then 2 kg of pretreated pulp and 100 L of water were added into the 105 L chamber of the TGCXZ-100 circulated ultrasonic apparatus (Hongxianglong Biotechnology Co. Ltd., Beijing, China). The apparatus was equipped with three 25 mm cylindrical titanium alloy probes. The ultrasonic frequency was set to 20 kHz, the output power was 800 W for each ultrasonic generator, the mechanical stirring speed was 600 rpm, and the processing time was 30 min.

Characterization. TEM images were collected using a JEM-2100 microscope (JEOL, Tokyo, Japan). FTIR spectra were recorded using a Nicolet 6700 FTIR spectrometer over the range of 4000 – 400 cm^{-1} (Thermo Fisher Scientific Inc., USA). The zeta potential was tested by the Zetasizer Nano ZS90 analyzer (Malvern Company, Worcestershire, UK). Solid-state nuclear magnetic resonance spectra were detected on a Brucker 400M spectrometer (Bruker, Ettlingen, Germany). Raman imaging was performed using a WITec Alpha300RA Confocal Raman microscope equipped with a charge-coupled device detector. Raman images were based on the integral band of ester group at 1740 cm^{-1} and hydroxyl group at 3400 cm^{-1}. The X-ray photoelectron spectroscopy (XPS) experiments were referenced to the C 1s neutral carbon peak at 284.8 eV. A K-Alpha system (Thermo Fisher Scientific, Basingstoke, UK) was used to analyze the bonding information of the sample. The X-ray diffraction (XRD) patterns were obtained with an X-ray diffractometer (XRD-6100, Rigaku, Shimadzu, Japan) with a copper target at 40 kV and 30 mA. The scanning angle range was 5–50°, and the scanning speed was 3°/min. Thermal conductivity of the

aerogel was calculated using the transient hot wire method at 25 °C on a thermal constant analyzer (TC3000E, XIATECH, Xian, China). The thermogravimetric analysis was performed using a STA 6000-SQ8 synchronous thermal analysis infrared spectrometer at a heating rate of 5 °C/min over a range of 25–700 °C under a nitrogen atmosphere. The mechanical properties of the film samples (20 mm × 5 mm × 1 mm) were tested by an Instron 5569 universal mechanical experimental machine at room temperature, with a tensile rate of 10 mm/min.

Determination of carboxyl content. The total carboxyl content (TCC) of C-CNFs was determined by alkaline hydrolysis and reverse titration. 0.5 g of sample was added to 40 mL (70%) ethanol solution, and the suspension was stirred for 30 min. Then 20 mL (0.5 M) NaOH solution was added to the suspension and hydrolyzed at 60 °C for 48 h. Phenolphthalein was used as an indicator to titrate unconsumed NaOH after hydrolysis with HCl (0.5 M) solution:

$$Total\,carboxyl\,content = \frac{C_{HCl} \times (V_B - V_S)}{m}$$

where C_{HCl}: the exact concentration of HCl solution (mol/l), V_B: HCl volume used for titration of blank samples, V_S: the exact volume of HCl solution used for C-CNF titration, m: the dry weight of C-CNF (g).

The free carboxyl content (FCC) of C-CNFx was determined by conductance titration. Fifty milligrams of C-CNF suspensions were selected, then 10 mL (0.01 M) HCl was added, and ultrasonic treatment was conducted for 4 h. Finally, the suspension was titrated with NaOH (0.01 M).

$$Free\,carboxyl\,content = \frac{C_{NaOH} \times V_{NaOH}}{m}$$

where C_{NaOH}: concentration of NaOH (0.01 M), V_{NaOH}: the volume of NaOH required to titrate all HCl, m: the dry weight of C-CNFs.

Detection of degree of substitution (DS). The DS of C-CNF sample was calculated according to the above two titrations.

$$DS = \frac{162.14 \times C_{HCl} \times (V_B - V_S) \times (1 - FC)}{m - C_{HCl} \times (V_B - V_S) \times (1 - FC) \times (192.13 - 18.02)}$$

where FC: ratio of free carboxyl content to total carboxyl content (FCC/TCC). The molecular weight of citric acid is 192.13 g/mol.

Calculation of DP. The specific viscosity of the sample dissolved in copper amine standard solution was measured by Ubbelohde viscometer (capillary diameter 0.80 mm, measuring ball solvent 4 mL). The DP of the sample was calculated according to a formula, and the average value was obtained by measuring five times. See ISO 5351 – 2010 for the details.

$$\eta = \frac{t - t_0}{t_0}$$

$$DP = \frac{\eta}{0.005 \times C(1 + 0.29\eta)}$$

where DP: average degree of polymerization, η: specific viscosity, t: time (s) for the cellulose/ cupriamine solution to flow through two scales of the viscometer, t_0: time (s) for blank cupriamine solution to flow through two scales of the viscometer, C: mass concentration of cellulose/ cupriamine solution (g/L).

Porosity calculation. Ignoring the air density inside the aerogel, the porosity was calculated as follows:

$$P\,(\%) = (1 - \frac{d_a}{d_n}) \times 100\%$$

where P: the porosity of the aerogel, d_a: density of the aerogel, and d_n: density of cellulose (~ 1.6 g/cm^3).

Declarations

Data availability

Data are available on reasonable request from the authors, according to their contributions.

Acknowledgements

Author contributions

H.Y. and K.Z. conceived the concept. X.S. and Z.W. performed most of the experiments. X.S., Z.W., H.Y. and K.Z. co-wrote the paper. Q.X., Y.L., W.C., and K.Z. participated in analysis of the results. All authors contributed to the general discussion and reviewing of the manuscript.

Competing interests

The authors declare that they have no competing interests.

Additional information

Supplementary information The online version contains supplementary material available at

Correspondence and requests for materials should be addressed to

References

1. Li T, *et al.* Developing fibrillated cellulose as a sustainable technological material. Nature. **590**, 47−56 (2021).
2. Ling S, Kaplan DL, Buehler MJ. Nanofibrils in nature and materials engineering. Nature Reviews Materials. **3**, 1−15 (2018).
3. Guan Q-F, *et al.* Lightweight, tough, and sustainable cellulose nanofiber-derived bulk structural materials with low thermal expansion coefficient. Science advances. **6**, eaaz1114 (2020).
4. Wu N, Zeng Z, Kummer N, Han D, Zenobi R, Nyström G. Ultrafine cellulose nanofiber-assisted physical and chemical cross-linking of MXene sheets for electromagnetic interference shielding. Small Methods. **5**, 2100889 (2021).
5. Li T, *et al.* A nanofluidic ion regulation membrane with aligned cellulose nanofibers. Science advances. **5**, eaau4238 (2019).
6. Isogai A, Hänninen T, Fujisawa S, Saito T. Catalytic oxidation of cellulose with nitroxyl radicals under aqueous conditions. Progress in Polymer Science. **86**, 122−148 (2018).
7. Chu Y, Sun Y, Wu W, Xiao H. Dispersion properties of nanocellulose: a review. Carbohydrate polymers. **250**, 116892 (2020).
8. Isogai A, Saito T, Fukuzumi H. TEMPO-oxidized cellulose nanofibers. nanoscale. **3**, 71−85 (2011).
9. Thomas B, Raj MC, Joy J, Moores A, Drisko GL, Sanchez C. Nanocellulose, a versatile green platform: from biosources to materials and their applications. Chemical reviews. **118**, 11575−11625 (2018).
10. Ji H, Xiang Z, Qi H, Han T, Pranovich A, Song T. Strategy towards one-step preparation of carboxylic cellulose nanocrystals and nanofibrils with high yield, carboxylation and highly stable dispersibility using innocuous citric acid. Green Chemistry. **21**, 1956−1964 (2019).
11. Spinella S, *et al.* Concurrent cellulose hydrolysis and esterification to prepare a surface-modified cellulose nanocrystal decorated with carboxylic acid moieties. ACS Sustainable Chemistry & Engineering. **4**, 1538−1550 (2016).
12. Beaumont M, *et al.* Assembling native elementary cellulose nanofibrils via a reversible and regioselective surface functionalization. Journal of the American Chemical Society. **143**, 17040−17046 (2021).
13. Yang CQ, Wang X. Formation of five-membered cyclic anhydride intermediates by polycarboxylic acids: thermal analysis and fourier transform infrared spectroscopy. Journal of applied polymer science. **70**, 2711−2718 (1998).
14. Shinoda R, Saito T, Okita Y, Isogai A. Relationship between length and degree of polymerization of TEMPO-oxidized cellulose nanofibrils. Biomacromolecules. **13**, 842−849 (2012).

15. Saito T, Kimura S, Nishiyama Y, Isogai A. Cellulose nanofibers prepared by TEMPO-mediated oxidation of native cellulose. Biomacromolecules. **8**, 2485–2491 (2007).

16. Zhu L, *et al.* Shapeable fibrous aerogels of metal–organic-frameworks templated with nanocellulose for rapid and large-capacity adsorption. ACS nano. **12**, 4462–4468 (2018).

17. Li D, Henschen J, Ek M. Esterification and hydrolysis of cellulose using oxalic acid dihydrate in a solvent-free reaction suitable for preparation of surface-functionalised cellulose nanocrystals with high yield. Green Chemistry. **19**, 5564–5567 (2017).

18. Rietzler B, Ek M. Adding value to spruce bark by the isolation of nanocellulose in a biorefinery concept. ACS Sustainable Chemistry & Engineering. **9**, 1398–1405 (2021).

19. Bian H, *et al.* Recyclable and reusable maleic acid for efficient production of cellulose nanofibrils with stable performance. ACS Sustainable Chemistry & Engineering. **7**, 20022–20031 (2019).

20. Wang R, Chen L, Zhu J, Yang R. Tailored and integrated production of carboxylated cellulose nanocrystals (CNC) with nanofibrils (CNF) through maleic acid hydrolysis. ChemNanoMat. **3**, 328–335 (2017).

21. Chen L, Zhu J, Baez C, Kitin P, Elder T. Highly thermal-stable and functional cellulose nanocrystals and nanofibrils produced using fully recyclable organic acids. Green Chemistry. **18**, 3835–3843 (2016).

22. Luo Y, *et al.* Preliminary investigations of the mechanisms involved in the ultrasonication-assisted production of carboxylic cellulose nanocrystals with different structural carboxylic acids. ACS Sustainable Chemistry & Engineering. **9**, 4531–4542 (2021).

23. Saini A, Yadav C, Xue B-L, Wang N, Dai L, Li X. Mixed-acid-assisted hydrothermal process for simultaneous preparation and carboxylation of needle-shaped cellulose nanocrystals. ACS Applied Polymer Materials. **2**, 548–562 (2019).

24. Yu H, Abdalkarim SYH, Zhang H, Wang C, Tam KC. Simple process to produce high-yield cellulose nanocrystals using recyclable citric/hydrochloric acids. ACS Sustainable Chemistry & Engineering. **7**, 4912–4923 (2019).

25. Yu H-Y, Zhang D-Z, Lu F-F, Yao J. New approach for single-step extraction of carboxylated cellulose nanocrystals for their use as adsorbents and flocculants. ACS Sustainable Chemistry & Engineering. **4**, 2632–2643 (2016).

26. Jiang J, *et al.* High production yield and more thermally stable lignin-containing cellulose nanocrystals isolated using a ternary acidic deep eutectic solvent. ACS Sustainable Chemistry & Engineering. **8**, 7182–7191 (2020).

27. Sirvio JA, Visanko M, Liimatainen H. Acidic deep eutectic solvents as hydrolytic media for cellulose nanocrystal production. Biomacromolecules. **17**, 3025–3032 (2016).

28. Ji Q, Yu X, Yagoub AE-GA, Chen L, Zhou C. Efficient cleavage of strong hydrogen bonds in sugarcane bagasse by ternary acidic deep eutectic solvent and ultrasonication to facile fabrication of cellulose nanofibers. Cellulose. **28**, 6159–6182 (2021).

29. Sehaqui H, Kulasinski K, Pfenninger N, Zimmermann T, Tingaut P. Highly carboxylated cellulose nanofibers via succinic anhydride esterification of wheat fibers and facile mechanical disintegration. Biomacromolecules. **18**, 242–248 (2017).

30. Song Y, Chen W, Niu X, Fang G, Min H, Pan H. An energy-efficient one-pot swelling/esterification method to prepare cellulose nanofibers with uniform diameter. ChemSusChem. **11**, 3714–3718 (2018).

31. Khanjanzadeh H, Park B-D. Optimum oxidation for direct and efficient extraction of carboxylated cellulose nanocrystals from recycled MDF fibers by ammonium persulfate. Carbohydrate Polymers. **251**, 117029 (2021).

32. Beaumont M, *et al.* Unique reactivity of nanoporous cellulosic materials mediated by surface-confined water. Nature communications. **12**, 1–8 (2021).

33. Yang X, Reid MS, Olsén P, Berglund LA. Eco-friendly cellulose nanofibrils designed by nature: effects from preserving native state. ACS nano. **14**, 724–735 (2019).

34. Jung YH, *et al.* High-performance green flexible electronics based on biodegradable cellulose nanofibril paper. Nature communications. **6**, 1–11 (2015).

35. Zhu H, *et al.* Anomalous scaling law of strength and toughness of cellulose nanopaper. *Proceedings of the National Academy of Sciences.* **112**, 8971–8976 (2015).
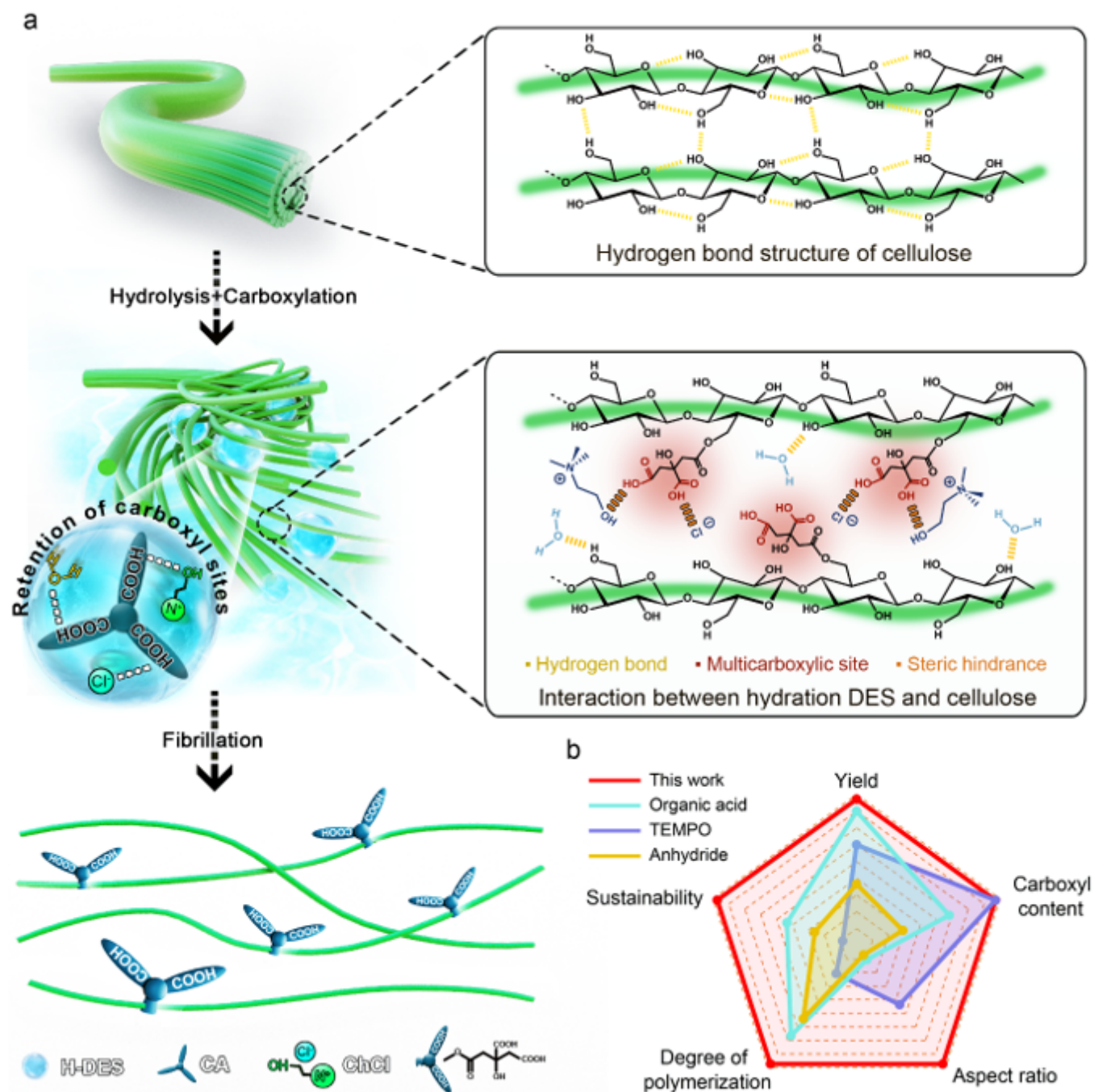
Figures

Figure 1

(a) Schematic illustration of the production of carboxylated cellulose nanofibers with high aspect ratios and rich carboxyl groups using a hydrated multi-carboxylic acid deep eutectic solvent. (b) A radar chart illustrates the advantages of the H-DES method presented in this work.

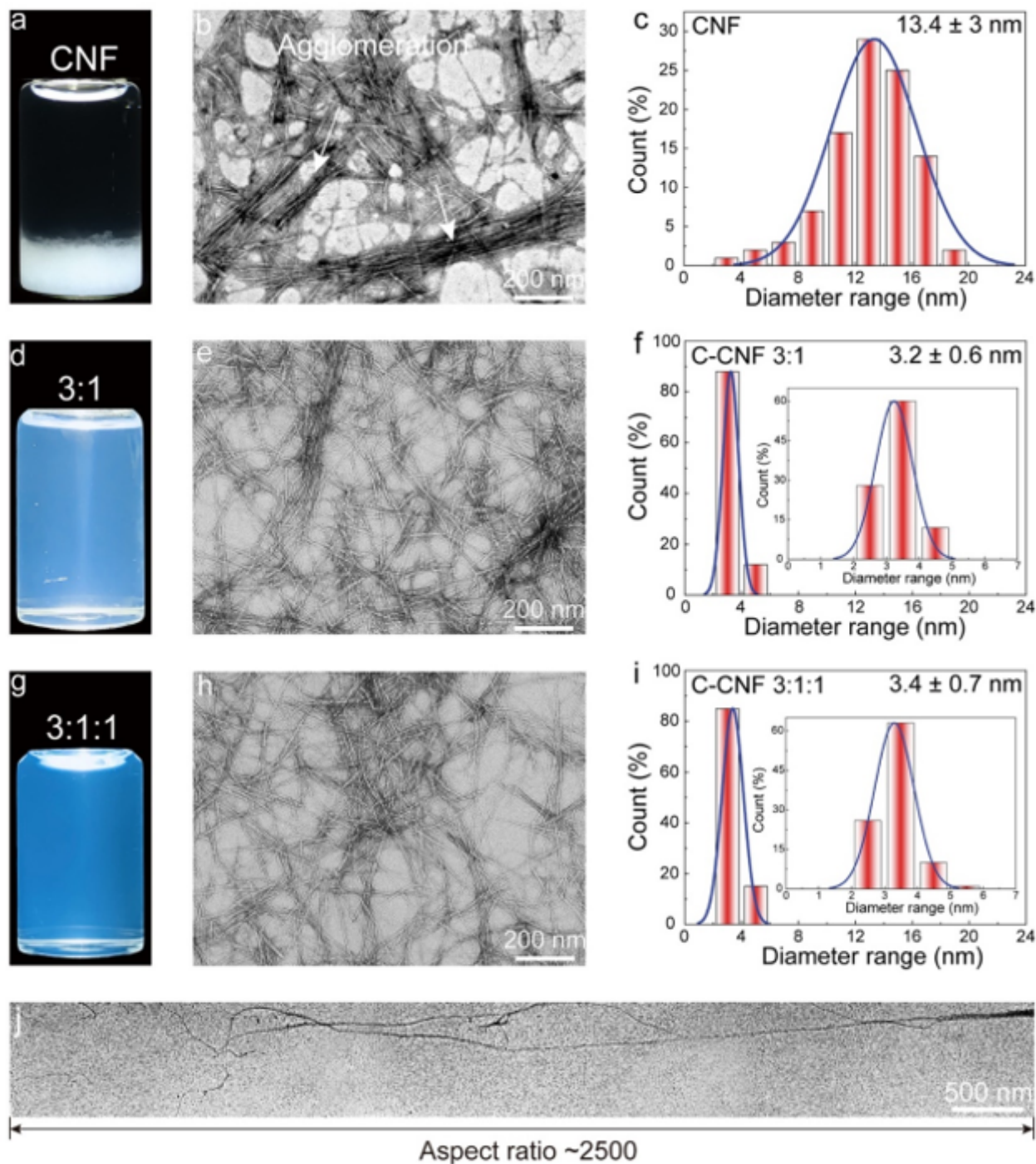**Figure 2**

Morphological characterizations of CNFs and C-CNFs. **(a)** Digital photographs, **(b)** TEM image, and **(c)** diameter distribution histogram of 0.2% (w/v) CNFs. **(d)** Digital photographs, **(e)** TEM image, and **(f)** diameter distribution histogram of 0.2% (w/v) C-CNFs by H-DES (CA:ChCl=3:1). **(g)** Digital photographs, **(h)** TEM image, and **(i)** diameter distribution histogram of 0.2% (w/v) C-CNFs by H-DES (CA:ChCl:H$_2$O=3:1:1); **(j)** the TEM image shows high length and high aspect ratio of typical C-CNFs by H-DES (CA:ChCl:H$_2$O=3:1:1).
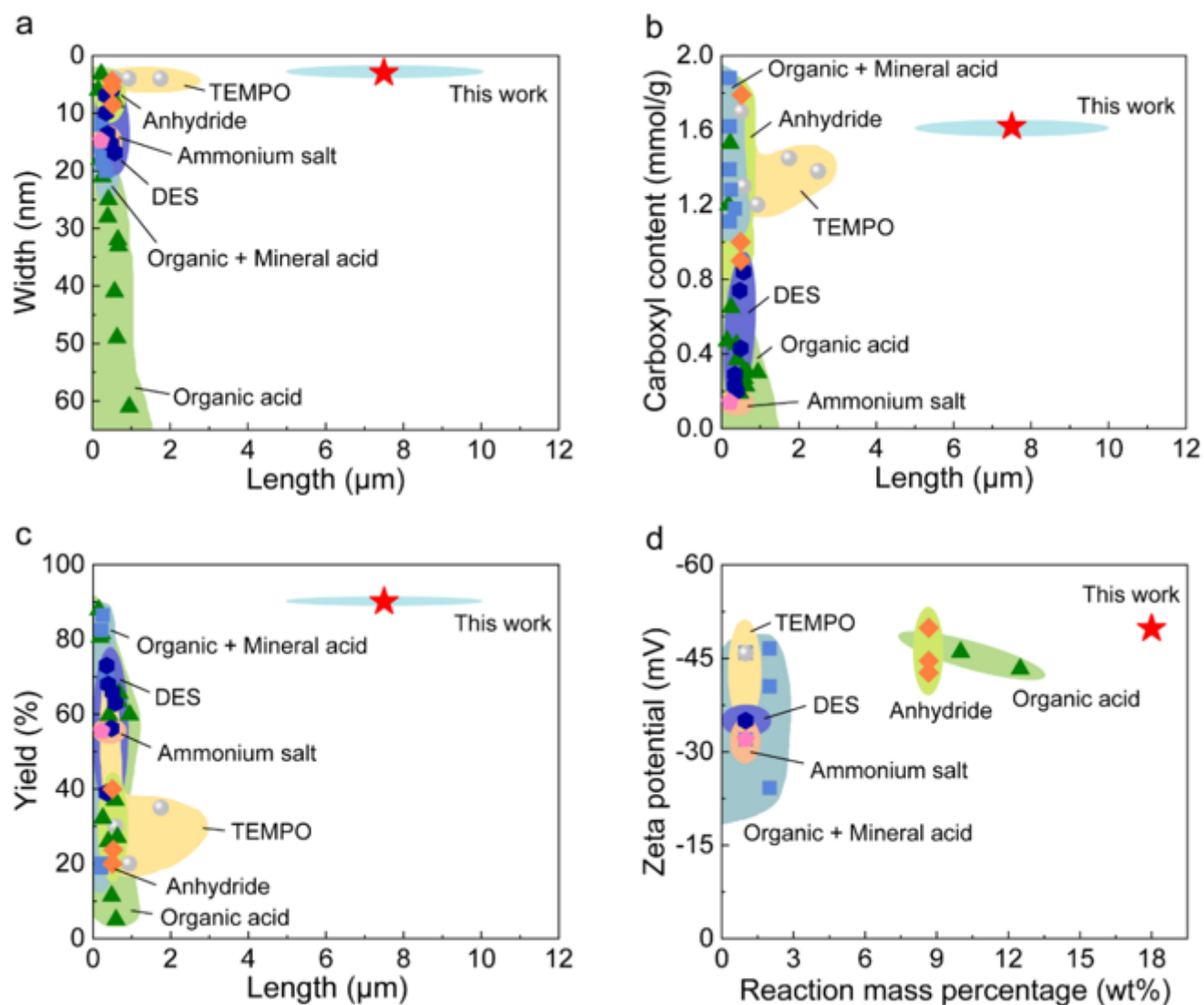
Figure 3

Ashby diagrams of **(a)** width versus length, **(b)** carboxyl content versus length, **(c)** yield versus length, and **(g)** zeta potential versus reaction mass percentage of C-CNFs prepared in this work and other reported works. The data used are summarized in Supplementary Table S1.[10-11, 14-31]
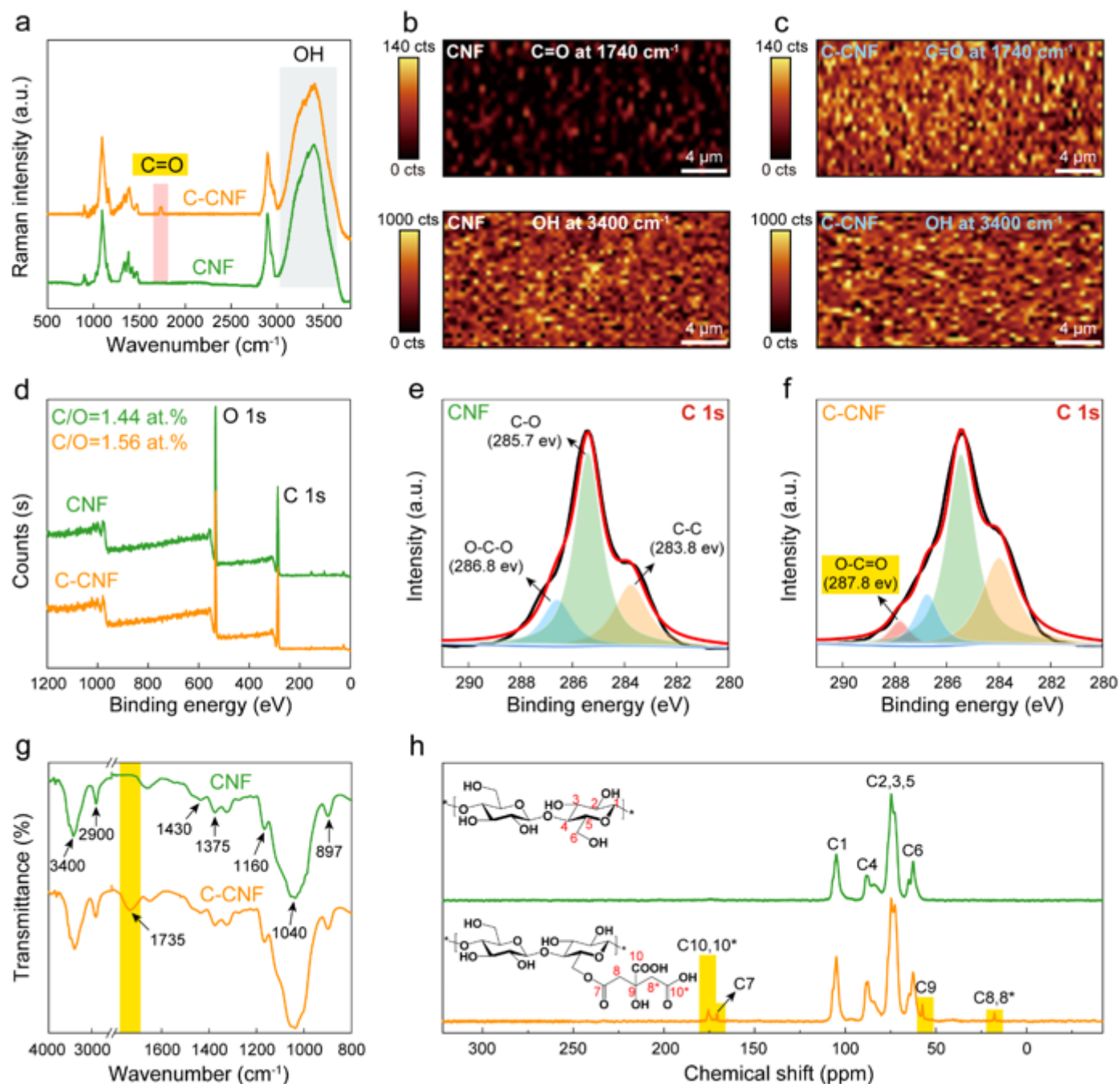
Figure 4

Chemical structure and state of CNFs and C-CNFs. (a) Raman spectra, Raman chemical mapping images of **(b)** CNFs and **(c)** C-CNFs; **(d)** XPS spectra, C 1s spectra of **(e)** CNFs and **(f)** C-CNFs; **(g)** FTIR spectra and **(h)** ^{13}C NMR spectra of CNFs and C-CNFs.
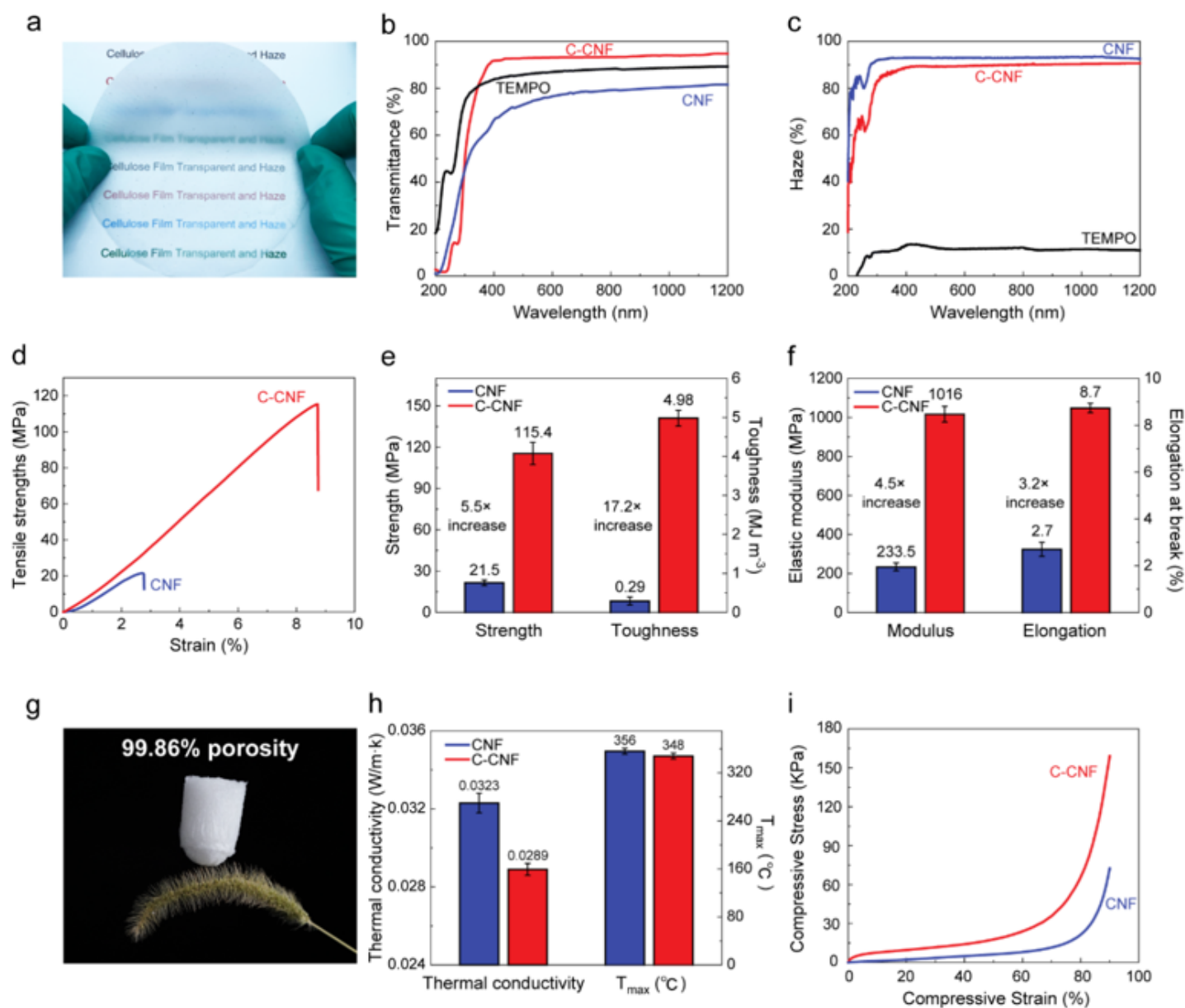
Figure 5

Physical and mechanical properties of C-CNF materials. (a) Photograph of the C-CNF film. **(b)** UV−vis transmittance and **(c)** haze spectra of the C-CNF film, with the CNF film and TEMPO-CNF film as controls. **(d)** Tensile stress-strain curves of the CNF film and C-CNF film. **(e)** Strength and toughness and **(f)** elastic modulus and elongation at break of the CNF film and C-CNF film. **(g)** Photograph of the ultralight C-CNF aerogel. **(h)** Thermal conductivity and stability and **(i)** compressive stress-strain curves of the CNF aerogel and C-CNF aerogel.
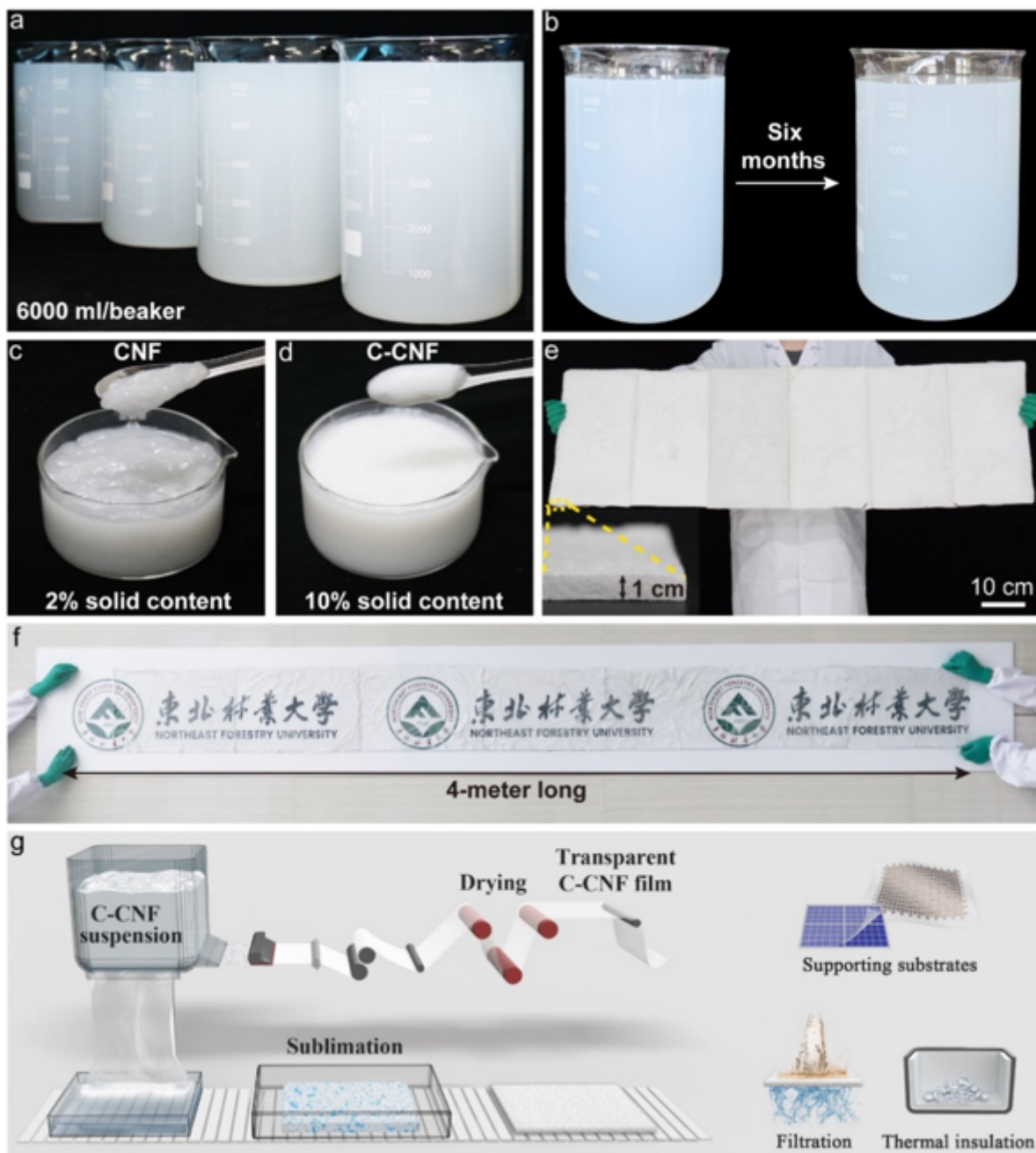
Figure 6

Scalable productivity of C-CNFs and their derived materials. (a) C-CNF suspension from scaling up production of 100 L per batch. **(b)** The C-CNF suspension before and after six months of deposit. Photographs of **(c)** 2 wt% CNFs and **(d)** 10 wt% C-CNFs. Photographs of **(e)** large bulk C-CNF aerogel and **(f)** meters-long C-CNF film. **(g)** Schematic illustration of the large-scale productivity of C-CNF derived materials.

Supplementary Files

This is a list of supplementary files associated with this preprint. Click to download.

- SupportingInformation.docx